Title

Altered canalicular remodeling associated with femur fracture in mice

Journal

Journal of Orthopaedic Research®, 40(4)

ISSN

0736-0266

Authors

Emami, Armaun J
Sebastian, Aimy
Lin, Yu-Yang
et al.

Publication Date

2022-04-01

DOI

10.1002/jor.25119

Peer reviewed

HHS Public Access

Author manuscript

J Orthop Res. Author manuscript; available in PMC 2023 April 01.

Published in final edited form as:

J Orthop Res. 2022 April ; 40(4): 891–900. doi:10.1002/jor.25119.

Altered canalicular remodeling associated with femur fracture in mice

Armaun J. Emami[1], **Aimy Sebastian**[2], **Yu-Yang Lin**[1], **Cristal S. Yee**[3], **Benjamin Osipov**[1], **Gabriela G. Loots**[2], **Tamara Alliston**[3], **Blaine A. Christiansen**[1]

[1]:University of California Davis Health, Department of Orthopaedic Surgery

[2]:Lawrence Livermore National Laboratory, Physical & Life Sciences Directorate

[3]:University of California San Francisco, Department of Orthopaedic Surgery

Abstract

We previously showed that femur fracture in mice caused a reduction in bone volume at distant skeletal sites within 2 weeks post-fracture. Osteocytes also have the ability to remodel their surrounding bone matrix through perilacunar/canalicular remodeling (PLR). If PLR is altered systemically following fracture, this could affect bone mechanical properties and increase fracture risk at all skeletal sites. In this study, we investigated whether lacunar-canalicular microstructure and the rate of PLR are altered in the contralateral limb following femoral fracture in mice. We hypothesized that femoral fracture would accelerate PLR by 2 weeks post-fracture, followed by partial recovery by 4 weeks. We used histological evaluation and high-resolution micro-computed tomography to quantify the morphology of the lacunar-canalicular network at the contralateral tibia, and we used quantitative RT-PCR and RNA-seq to measure expression of PLR-associated genes in the contralateral femur. We found that at both 2 and 4 weeks post-fracture, canalicular width was significantly increased by 18.6% and 16.6%, respectively, in fractured mice relative to unfractured controls. At 3 days and 4 weeks post-fracture, we observed down-regulation of PLR-associated genes; RNA-seq analysis at 3 days post-fracture showed a deceleration of bone formation and mineralization in the contralateral limb. These data demonstrate notable canalicular changes following fracture that could affect bone mechanical properties. These findings expand our understanding of systemic effects of fracture and how biological and structural changes at distant skeletal sites may contribute to increased fracture risk following an acute injury.

Keywords

Fracture Healing; Perilacunar/Canalicular Remodeling (PLR); μCT; Bone Histomorphometry; Osteocytes

Correspondence: Blaine A. Christiansen, Ph.D., University of California Davis Health, Department of Orthopaedic Surgery, 4635 2nd Ave, Suite 2000, Sacramento, CA 95817, Phone: 916-734-3974, Fax: 916-734-5750, bchristiansen@ucdavis.edu.

Introduction

There are over 2 million osteoporosis-related fractures annually in the United States, which account for over 19 billion dollars in medical related costs [1]. Predicting and preventing osteoporotic fractures is therefore a major health concern. One of the most reliable predictors of fracture risk is a previous fracture of any kind [2–8]. In a previous study, we showed that femur fracture in mice caused reduced bone volume at a distant skeletal site (lumbar spine) within 2 weeks post-fracture; this bone loss was associated with increased osteoclast number, systemic inflammation, and decreased voluntary activity at early time points (3–4 days post-fracture) [9]. This suggests that the healing response to a fracture may involve processes that decrease bone mass systemically, and this decreased bone mass may increase the risk of subsequent fractures.

Osteocytes have the ability to directly resorb their surrounding bone matrix through perilacunar/canalicular remodeling (PLR); this process is a mechanism of mineral mobilization during processes such as lactation [10, 11]. For example, after 12–14 days of lactation in mice, lacunar area increased 7–30%, and canalicular width increased 15–50% [10, 11]. Several genes that are commonly associated with osteoclastic bone resorption are upregulated in osteocytes during PLR, including tartrate resistant acid phosphatase 5 (*Acp5*), cathepsin K (*Ctsk*), carbonic anhydrase 1 (*Car1*), carbonic anhydrase 2 (*Car2*), Na+/H+ exchanger domain containing 2 (*Nhedc2*), ATPase H+ transporting lysosomal V1 subunit G1 (*ATP6b1g1*), ATPase H+ transporting lysosomal V0 subunit D2 (*ATP6v0d2*), and matrix metallopeptidase 13 (*Mmp13*) [11]. It is currently unknown whether PLR by osteocytes is altered systemically following a bone fracture, and if so, whether this process occurs by the same mechanisms and with a similar time course as other conditions that initiate PLR such as lactation.

The goal of this study was to determine whether PLR is altered at distant skeletal sites following femur fracture in mice. We quantified lacunar-canalicular morphology in the contralateral limb using histological analysis and high-resolution micro-computed tomography, and quantified biomarkers of PLR using RT-PCR and RNA sequencing (RNA-seq). We hypothesized that femoral fracture in mice would accelerate PLR at early time points post-fracture (<2 weeks), potentially as a mechanism for utilizing mineral stores from the skeleton for formation of the fracture callus, followed by partial recovery at later time points. These results would provide evidence in support of PLR as a mechanism by which an initial fracture systemically weakens the skeleton and increases the risk for subsequent fractures by negatively affecting bone quality and whole-bone mechanical properties throughout the skeleton.

Materials and Methods

Animals

A total of 65 mice (12-week-old male C57BL/6J; The Jackson Laboratory, Bar Harbor, ME) were used for this study and were randomly assigned to experimental groups. Fractured mice were subjected to stabilized transverse femur fracture (described in more detail below), while Control mice were subjected to anesthesia and analgesia only (no surgical

procedures). Thirty-one mice were euthanized at 2 or 4 weeks post-fracture for histological analysis of lacunar-canalicular morphology in the contralateral tibia, RT-PCR analysis of PLR biomarkers in the contralateral femur, and micro-computed tomography (μCT) analysis of trabecular bone microstructure in the L5 vertebral body (n = 7–8 per group). Eighteen mice were euthanized at 2 weeks or 4 weeks post-fracture for high-resolution μCT analysis of the contralateral tibia (n = 4–6 per group). Fourteen mice (n = 7 per group) were euthanized 3 days post-fracture for RNA-seq analysis of the contralateral femur. Investigators were blinded to experimental groups during all analyses. Animal numbers and group sizes were chosen based on data from our previous study [9]. Two mice were euthanized immediately after fracture surgery due to intramedullary pin misplacement or complications after surgery. Mice were cared for in accordance with the guidelines set by the National Institutes of Health (NIH) on the care and use of laboratory animals. All procedures were approved by the Institutional Animal Care and Use Committee of the University of California Davis.

Creation of Transverse Femur Fracture

All mice were anesthetized with isoflurane inhalation, and received a pre-operative dose of buprenorphine (0.05 mg/kg). For Fractured mice, an incision was created on the lateral side of the right knee, and a 0.01 in. stainless steel wire pin was inserted into the medullary canal as originally described by Bonnarens and Einhorn [12]. Stabilized transverse fractures were created with a controlled lateral impact using a modified fracture apparatus [13, 14]. Immediately post-fracture, mice were imaged with planar radiographs (HE100/30+ X-ray machine, MinXRay, Northbrook IL) with a CXD1–31 plate (Canon, Lake Success, NY) to confirm pin positioning and a transverse mid-diaphyseal fracture. Full weight-bearing and unrestricted activity were permitted post-operatively.

Micro-Computed Tomography Analysis of Trabecular Bone

Following dissection, L5 vertebrae were preserved in 70% ethanol, and were imaged using micro-computed tomography (SCANCO Medical, μCT 35, Brüttisellen, Switzerland) to quantify trabecular bone microstructure in the vertebral body. During imaging, bones were embedded in 1.5% agarose to hold them stationary and to provide hydration, and were scanned with a 6 μm isotropic nominal voxel size (x-ray tube potential = 55 kVp, current = 114 μA, integration time = 900 ms) according to the JBMR guidelines for μCT analysis of rodent bone structure [15]. Volumes of interest for trabecular bone in the L5 vertebral body were manually contoured on transverse images, excluding the cortical shell and the transverse processes, and extending from the cranial growth plate to the caudal growth plate. Trabecular bone volume fraction (BV/TV), bone tissue mineral density (TMD) and other microstructural outcomes were determined using the manufacturer's analysis software. A threshold of 562.8 mg HA/cm^3 was used to segment "bone" from "non-bone" voxels.

Silver Nitrate Staining Analysis of Lacunar and Canalicular Microstructure

Tibias were fixed in 4% paraformaldehyde for 48 hrs, and were then decalcified in 0.34 M EDTA for 14 days with solution changes every 2–3 days followed by serial ethanol dehydration. Tibias were embedded in paraffin, and 5 μm transverse sections were taken at 30% length from the proximal end of the tibia. To visualize the osteocyte lacunocanalicular

network, sections were deparaffinized and incubated in two-parts 50% silver nitrate and one-part 1% formic acid in 2% gelatin solution for 55 minutes, as previously described [16]. Stained slides were washed in 5% sodium thiosulfate for 10 minutes and subsequently dehydrated, cleared, and mounted. Images were acquired at 100x for analysis using a Nikon Eclipse E800 bright-field microscope. Images were obtained in each quadrant of the tibia transverse sections per section (four images per section), 3–5 sections per sample.

Canicular width, canalicular length, lacunar area, and number of canaliculi per lacuna were analyzed with ImageJ. Canalicular width was measured using the Sharpen and Find Edges features, by drawing lines across the canalicular walls at multiple locations. An average of 5 width measurements were made on 4–6 canaliculi per lacuna; canalicular length was measured on all canaliculi, and 36–50 lacunae were measured for each tibia. For each canalicular width measurement, a grey scale plot was generated, and the distance was measured between one-third of the distance from the bottom of each left and right peak, which was the approximate transition point from white to dark pixels based on visual inspection of the canaliculi. All measurements were averaged to determine the mean canalicular width, canalicular length, and number of canaliculi per lacuna for each mouse. Lacunar area was measured by processing images into a gray-scale image, then binary image, and manually circling each lacuna. For each image, lacunar area was calculated using ImageJ Analyze Particles feature to obtain total lacunar area per image. For each tibia, the average lacunar area represents data from 4 images per section, 3–5 sections per tibia.

High-Resolution μCT Measurement of Lacunar Volume

Bones were scanned using high-resolution μCT (Xradia, MicroXCT-200, Carl Zeiss X-ray Microscopy, Inc., Pleasanton, CA) with 1.1035 μm nominal voxel size (x-ray tube potential = 80 kVp, current = 100 μA), filter for 20x of 0.14–0.08 transmission (LE #6). The scan region of interest was a 1 mm^3 cubic volume that contained both cortical and trabecular regions on the anterior side of the proximal tibia. All analyses were performed using Amira analysis software (Thermo Fisher Scientific, Berlin, Germany). Lacunae in trabecular bone and cortical bone were analyzed separately. Lacunae were identified as porosities with a volume size of 100–800 μm^3 [17, 18]. Total lacunar volume per bone volume and average lacunar volume were determined for each of the trabecular and cortical regions.

RT-PCR Analysis of PLR Biomarkers

For mice euthanized at 2 or 4 weeks post-fracture (n = 31), the contralateral femur was extracted, epiphyses and periosteum were removed, bone marrow was flushed by low speed centrifugation (7,000 rpm) [19], cortical bone regions were flash-frozen in liquid nitrogen and homogenized in TRIzol (Invitrogen, Carlsbad, CA) as previously described [20]. Briefly, mRNA was purified using the RNeasy Mini Kit following manufacturer's instructions (Qiagen). RNA was reverse-transcribed using the iScript cDNA synthesis kit. qPCR was performed using iQ SYBR Green Supermix (BioRad) for beta-actin (*β-actin*), matrix metallopeptidase 2 (*Mmp2*), matrix metallopeptidase 13 (*Mmp13*), sclerostin (*Sost*), receptor activator of nuclear kappa B ligand (*RankL*), osteoprotegerin (*Opg*), carbonic anhydrase 2 (*Car2*), and ATPase H+ transporting lysosomal V0 subunit D2 (*ATP6v0d2*), with *β-actin* as the housekeeping gene. Expression was quantified by the ΔΔCT method

[21]. *Mmp2* and *Mmp13* expression is increased during remodeling of the extracellular matrix during PLR [22], *Sost* is an inhibitor of bone formation and a late marker of mature osteocytes [23], *RankL* is a positive regulator of osteoclastogenesis [24, 25], *Opg* is a secreted antagonist of *RankL* signaling [25], and *Car2* and *ATP6v0d2* are associated with proton pumps or acidification of the matrix during osteoclastic resorption and by osteocytes during PLR [11].

RNA-seq

Fourteen mice (7 Fractured, 7 Control) were euthanized at 3 days post-fracture, the contralateral femur was extracted, the epiphyses and periosteum were removed, and bone marrow was flushed by low speed centrifugation (7,000 rpm). Femoral cortices were then flash-frozen in liquid nitrogen and processed using TRIzol (Invitrogen, Carlsbad, CA) according to the manufacturer's protocol. RNA was purified with a Zymo RNA clean & Concentrator kit (Zymo Research Corp., Irvine, CA). RNA-seq was run using a CORALL Total RNA-seq Library Prep Kit (Lexogen, Vienna, Austria). Raw reads were processed with HTStream (https://ibest.github.io/HTStream/) to remove phiX and adapter sequences, and to assess ribosomal RNA content using a set of mouse rRNA sequences. Processed reads were aligned to GRCm38.p6 primary genome assembly using GENCODE v21 annotation, with STAR v.2.7.0e, to generate counts per gene [26]. Prior to statistical analysis, genes with low expression were filtered. Unwanted variation in the data was estimated using RUVseq version 1.18.0 [27]. Differential expression analyses were conducted using edgeR version 3.26.8 [28], adjusting for factors of unwanted variation. Gene ontology (GO) enrichment analyses were conducted using DAVID version 6.8. Heatmaps were generated using gplots version 3.0.3 in R version 4.0.2.

Statistical Analysis

Statistical analyses were performed using JMP Pro 13.0.1 (SAS Institute Inc., Cary, NC). All results are expressed as mean ± standard deviation (SD). Most data were analyzed by two-way analysis of variance (ANOVA) with time point post-fracture and experimental group (Fractured or Control) as factors to determine main effects and interactions. Post-hoc analyses were performed using Tukey's Honest Significant Difference test. Statistically significant differences were identified at $p \leq 0.05$. Statistical trends were noted at $p \leq 0.10$.

Results

Micro-Computed Tomography Analysis of Trabecular Bone

Consistent with our previous study, femur fracture was associated with lower trabecular bone volume in the L5 vertebral body of mice (Fig. 1). Fractured mice had 9.6% lower trabecular bone volume fraction (BV/TV) than Control mice at 2 weeks post-fracture ($p = 0.079$), and 12.1% lower BV/TV than control mice at 4 weeks post-fracture ($p = 0.130$), though these differences were not statistically significant. No significant differences were observed between Fractured and Control mice for trabecular thickness (Tb.Th), trabecular number (Tb.N), or trabecular separation (Tb.Sp) at either time point. At 4 weeks post-fracture, Fractured mice exhibited at 1.8% decrease in bone TMD ($p = 0.006$), which could

potentially reflect changes in microporosities in the bone tissue. However, there was no significant difference in TMD between Fractured and Control mice at 2 weeks post-fracture.

Silver Nitrate Staining Analysis of Lacunar and Canalicular Microstructure

Femur fracture was associated with significant increases in canalicular width in cortical bone of the contralateral tibia (Fig. 2). Mean canalicular width was 18.6% and 16.6% greater in Fractured mice at 2 and 4 weeks post-fracture, respectively, relative to Control mice (Fig. 2C). In contrast, no significant differences were observed for canalicular length, number of canaliculi per lacuna, or lacunar area between Fractured and Control mice (Fig. 2D, G, H).

High-Resolution μCT Measurement of Lacunar Volume

Using high-resolution μCT imaging we were able to quantify the volume and morphology of individual lacunae in both cortical and trabecular bone of the proximal tibia. However, consistent with our results from histological analysis, no significant differences were observed between Control and Fractured mice for either total lacunar volume per bone volume or average lacunar volume at either time point (Fig. 3).

RT-PCR Analysis of PLR Biomarkers

Some significant differences in the expression of PLR-related genes were observed following femur fracture in mice, though these differences were not consistent with previous studies that described conditions of accelerated PLR [11], and were not the same at the two time points investigated in this study. No significant differences in the expression of any PLR-related genes were observed between the Control and Fractured mice at 2 weeks post-fracture. However, at 4 weeks post-fracture, expression of *Mmp13* and *ATP6v0d2* were significantly lower in Fractured mice compared to Control mice (−45.3% for *Mmp13*, −38.4% for *ATP6v0d2*, Fig. 4). Expression of *Sost*, *Opg*, *Car2*, and *Mmp2* were not statistically different between Control and Fractured groups at either time point.

RNA-seq

Analysis of contralateral femurs with RNA-seq at 3 days post-fracture yielded results that were consistent with those for RT-PCR analysis at 4 weeks post-fracture. Overall, 46 genes were upregulated and 318 genes were down-regulated in femurs from Fractured mice compared to those from Control mice (Table S1). Among the genes associated with PLR, expression of *Mmp2* and *Sost* was significantly lower in Fractured mice compared to Control mice. Gene ontology (GO) enrichment analyses of differentially expressed genes identified multiple biological processes associated with skeletal development and bone metabolism, immune/inflammatory responses, angiogenesis and response to hypoxia as enriched (Fig. 5, Table S2). Several key regulators of bone metabolism including *Col1a1*, *Col1a2*, *Bglap*, *Bmp1*, *Alpl*, *Mepe*, *Sost* and *Sfrp2* were among the top down-regulated genes (Fig. 5A). Several genes associated with B-cell/T-cell differentiation and function including *Cd19*, *Cd79b*, *Cd38*, *Cd74*, *H2-Aa*, *Cd3d*, *Rag1*, *Il7r* and *Il2ra* were also significantly down-regulated in Fractured mice compared to Control mice (Fig. 5B).

Discussion

In this study, we investigated biological and microstructural indicators of osteocytic perilacunar/canalicular remodeling in the contralateral limb following femur fracture in mice. Consistent with our initial hypothesis, we found that femur fracture was associated with significantly increased canalicular width at 2 and 4 weeks post-injury. However, contrary to our hypothesis, lacunar area, canalicular length, and number of canaliculi per lacuna were not changed following femur fracture, and genes that commonly have increased expression during PLR were down-regulated in contralateral limbs of Fractured mice. Therefore, although these data demonstrate notable canalicular changes following fracture that could affect whole-bone mechanical properties and fracture risk, the associated biological changes are not consistent with previous studies of PLR during conditions such as lactation.

Osteocytes play a crucial role in regulating bone mineral [23, 29–33]; this is underscored by the amount of bone surface area available to them. Lacunar-canalicular surfaces represent roughly one hundred times more surface area than osteoclasts' resorbing surfaces (i.e., haversian canals, Volkmann canals, cancellous bone) [23, 34]. In the current study, we observed considerable increases in canalicular width following fracture, but no significant changes in lacunar volume. This disproportionate change in canalicular morphology is consistent with previous studies that investigated perilacunar/canalicular remodeling in mice [10, 11, 20, 35]. For example, Kaya et. al. found that lactation induced a 7% increase in lacunar area, but a 15% increase in canalicular width; these changes in cortical bone tissue were also associated with a reduction in bone tissue-level elastic modulus [10]. Furthermore, the increased canalicular width is consistent with decreased tissue mineralization following fracture, as we observed with decreased μCT-derived TMD, even in the absence of changes in the microstructure of trabecular bone. However, we did not quantify canalicular dimensions in trabecular bone osteocytes in this study, so this association is currently speculative. Although we did not quantify bone mechanical properties in the current study, changes in canalicular width could affect cortical bone quality and whole-bone mechanical strength. Altogether, these data partially support the hypothesis that fracture alters the rate of PLR systemically, which contributes to increased fracture risk at all skeletal sites.

A previous study in lactating mice showed increased expression of *CA2*, *ATP6v0d2*, and *Mmp13*, associated with significant lacunar and canalicular microstructural changes at the 2 week time point [11]. Additionally, after 21 days of glucocorticoid treatment in mice (which suppresses PLR), histological analysis demonstrated a lower expression of *Mmp13* in treated mice [36]. Our quantification of RNA expression of PLR-associated genes found lower expression of *Mmp2* and *Sost* at 3 days post-fracture, no differences in PLR gene expression at 2 weeks post-fracture, and lower expression of *Mmp13* and *ATP6v0d2* at 4 weeks post-fracture, suggesting a possible suppression of PLR activity post-fracture, though RT-PCR data had high variability and may not be easily interpretable. Using RNA-seq we also observed altered gene expression patterns associated with bone formation, bone mineralization, and the inflammatory response, with the expression of associated genes typically being decreased in Fractured mice. However, interpretation of these data is challenging, as these changes may reflect the presence of other cell types in the collected

tissue (inflammatory cells, osteoblasts, osteoclasts, osteoprogenitors, fibroblasts, etc.), so we cannot conclude that these gene expression profiles are purely reflective of osteocyte activity. Instead, these data more generally describe the overall effect of fracture on the biology of the contralateral limb, which is inclusive of, but not exclusive to, PLR. Future work could more specifically investigate local gene expression changes in osteocytes using techniques such as immunohistochemistry or in situ hybridization for PLR-associated genes.

RNAseq data suggest an overall deceleration of bone turnover, or a reduction in anabolic output, in the contralateral limb following fracture, rather than the systemic acceleratory phenomenon that has previously been proposed [37, 38]. This deceleration is consistent with our previous study [9] that showed a decreased bone formation rate in the lumbar spine of mice at 4 and 6 weeks following femur fracture. The underlying mechanisms of this deceleration are currently unknown, but could be partially related to altered gait or decreased voluntary activity following femur fracture. In our previous study, we demonstrated decreased ambulatory time and decreased rearing activity in mice at day 3 post-fracture; these changes could potentially contribute to the downregulation of genes in the contralateral limb. However, contrary to this hypothesis, we also observed a reduction in Sclerostin in the contralateral limb post-fracture; downregulation of *Sost* is typically associated with an increased anabolic response and an increase in bone mass. Altogether, these data suggest that PLR is altered in the contralateral limb following a bone fracture, but these changes are dynamic, and the time points investigated in this study may not have captured the peak in the expression of resorption genes that correspond with the histological and μCT data.

Systemic bone loss following fracture, including altered canalicular microstructure, may be a mechanism of mineral recruitment for formation of the fracture callus. Bone is an endocrine organ that acts as a reservoir for mineral. Utilizing mineral stores from the entire skeleton to address an acute mineral need such as formation of a fracture callus may be an effective method for rapidly addressing an urgent need, but may also cause lasting effects of increased fracture risk at all skeletal sites, at least until bone mass is able to recover. Systemic bone loss as a method of mineral utilization is supported by studies that show improved fracture healing and reduced post-traumatic bone loss at distant skeletal sites with calcium supplementation in mice [39, 40]. Moreover, mice fed a calcium/vitamin-D deficient diet exhibited higher levels of bone resorption and lower bone mass at other skeletal sites post-fracture compared to mice on a normal diet. Altogether, these findings suggest that calcium mobilization during fracture callus formation may be an underlying mechanism of systemic bone loss following fracture. However, the current study did explicitly investigate this hypothesis, so this association remains to be established experimentally.

This study is the first to demonstrate changes in the canalicular network at a distant skeletal site following a bone fracture. We used multi-modal imaging methods to quantify lacunar-canalicular morphology, and generated considerable data describing the biological response to fracture in the contralateral limb. However, this study had some important limitations that must be acknowledged. First and foremost, different skeletal sites were used for different analyses (L5 vertebral body, femur, tibia), and it is possible that microstructural changes

and biological activity are not the same at different skeletal sites, particularly at axial vs. appendicular skeletal sites. Trabecular bone was analyzed at the L5 vertebral body in order to confirm the post-traumatic bone loss response that we observed at this site in our previous study [9]. However, the focus of the current study was on PLR by osteocytes, primarily in cortical bone, so the contralateral femur and tibia were used for most analyses. A more comprehensive analysis would have included both μCT assessment of bone microstructure and histological assessment of PLR at the same skeletal sites. Second, the femur fracture model used in this study can have some variability in fracture location and severity, which may affect systemic inflammation and activity levels post-injury. Next, in this study we did not directly measure bone formation or bone resorption rates, which could have provided more direct evidence of osteocytes' response after fracture. Additionally, our study used only young male mice, which makes it difficult to compare these results to previous studies of lactation in female mice (a common model of increased PLR), or to our previous study that used only female mice [9]. Also, in our previous study we showed that young mice fully recovered from the loss of bone volume by 6 weeks post-fracture, whereas older mice may have longer-lasting effects of systemic bone loss [9]. Time points longer than 4 weeks post-fracture could be investigated in order to fully understand the time course of bone loss and recovery in the lacunar-canalicular network.

Conclusion

In this study, we showed that femur fracture in mice initiated significant morphological changes in the canalicular network in the contralateral limb, which was associated with down-regulation of genetic biomarkers associated with PLR and a deceleration of bone formation and mineralization. It is possible that changes in canalicular remodeling by osteocytes are a process by which the mineral is utilized from the skeleton for callus formation and bone repair following a fracture, but this process may also lower bone quality and increase future fracture risk systemically. These findings expand our understanding of systemic effects of fracture and how biological and structural changes at distant skeletal sites may contribute to increased fracture risk following an acute injury.

Supplementary Material

Refer to Web version on PubMed Central for supplementary material.

Acknowledgments

We would like to thank the UC Davis Genome Center DNA Technologies and Expression Analysis Core (https://dnatech.genomecenter.ucdavis.edu/), supported by NIH Shared Instrumentation Grant S10 OD010786, for their assistance with RNAseq analysis. We would also like to acknowledge Douglas Rowland and the UC Davis Center for Molecular and Genomic Imaging (https://cmgi.ucdavis.edu/) for assistance with high-resolution imaging of lacunar morphology. Research reported in this publication was supported by the National Institute of Arthritis and Musculoskeletal and Skin Diseases, part of the National Institutes of Health, under Award Numbers R01 AR071459 (BAC) and P30 AR075055 (TA). AS and GGL conducted work under the auspices of the U.S. Department of Energy by Lawrence Livermore National Laboratory under Contract DE-AC52-07NA27344. The content is solely the responsibility of the authors. The funding body was not involved with design, collection, analysis, or interpretation of data; or in the writing of the manuscript. The authors have no conflicts of interest to disclose.

Disclosures:

Research reported in this publication was supported by the National Institute of Arthritis and Musculoskeletal and Skin Diseases, part of the National Institutes of Health, under Award Number R01 AR071459 (BAC) and P30 AR075055 (TA). The content is solely the responsibility of the authors. The funding bodies were not involved with design, collection, analysis, or interpretation of data; or in the writing of the manuscript. AS and GGL conducted work under the auspices of the U.S. Department of Energy by Lawrence Livermore National Laboratory under Contract DE-AC52-07NA27344. The authors have no conflicts of interest or financial ties to disclose.

REFERENCES

1. National Osteoporosis Foundation, “What Is Osteoporosis and What Causes It?”. Retrieved September 1, 2020, from National Osteoporosis Foundation Web site: https://www.nof.org/patients/what-is-osteoporosis/.
2. Clinton J, et al. , Proximal humeral fracture as a risk factor for subsequent hip fractures. J Bone Joint Surg Am, 2009. 91(3): p. 503–11. [PubMed: 19255209]
3. Klotzbuecher CM, et al. , Patients with prior fractures have an increased risk of future fractures: a summary of the literature and statistical synthesis. J Bone Miner Res, 2000. 15(4): p. 721–39. [PubMed: 10780864]
4. Wu F, et al. , Fractures between the ages of 20 and 50 years increase women’s risk of subsequent fractures. Arch Intern Med, 2002. 162(1): p. 33–6. [PubMed: 11784217]
5. Haentjens P, et al. , Colles fracture, spine fracture, and subsequent risk of hip fracture in men and women. A meta-analysis. J Bone Joint Surg Am, 2003. 85-A(10): p. 1936–43.
6. Lauritzen JB, et al. , Radial and humeral fractures as predictors of subsequent hip, radial or humeral fractures in women, and their seasonal variation. Osteoporosis International, 1993. 3(3): p. 133–137. [PubMed: 8481589]
7. Robinson CM, et al. , Refractures in patients at least forty-five years old. a prospective analysis of twenty-two thousand and sixty patients. J Bone Joint Surg Am, 2002. 84-A(9): p. 1528–33.
8. Johnell O, et al. , Fracture risk following an osteoporotic fracture. Osteoporos Int, 2004. 15(3): p. 175–9. [PubMed: 14691617]
9. Emami AJ, et al. , Age Dependence of Systemic Bone Loss and Recovery Following Femur Fracture in Mice. J Bone Miner Res, 2019. 34(1): p. 157–170. [PubMed: 30189111]
10. Kaya S, et al. , Lactation-Induced Changes in the Volume of Osteocyte Lacunar-Canalicular Space Alter Mechanical Properties in Cortical Bone Tissue. J Bone Miner Res, 2017. 32(4): p. 688–697. [PubMed: 27859586]
11. Qing H, et al. , Demonstration of osteocytic perilacunar/canalicular remodeling in mice during lactation. J Bone Miner Res, 2012. 27(5): p. 1018–29. [PubMed: 22308018]
12. Bonnarens F and Einhorn TA, Production of a standard closed fracture in laboratory animal bone. J Orthop Res, 1984. 2(1): p. 97–101. [PubMed: 6491805]
13. Toupadakis CA, et al. , Long-term administration of AMD3100, an antagonist of SDF-1/CXCR4 signaling, alters fracture repair. J Orthop Res, 2012. 30(11): p. 1853–9. [PubMed: 22592891]
14. Marturano JE, et al. , An improved murine femur fracture device for bone healing studies. Journal of Biomechanics, 2008. 41(6): p. 1222–1228. [PubMed: 18384794]
15. Bouxsein ML, et al. , Guidelines for assessment of bone microstructure in rodents using micro-computed tomography. J Bone Miner Res, 2010. 25(7): p. 1468–86. [PubMed: 20533309]
16. Yee CS, et al. , Investigating Osteocytic Perilacunar/Canalicular Remodeling. Curr Osteoporos Rep, 2019. 17(4): p. 157–168. [PubMed: 31227998]
17. Hemmatian H, et al. , Accuracy and reproducibility of mouse cortical bone microporosity as quantified by desktop microcomputed tomography. PLoS One, 2017. 12(8): p. e0182996. [PubMed: 28797125]
18. Dong P, et al. , 3D osteocyte lacunar morphometric properties and distributions in human femoral cortical bone using synchrotron radiation micro-CT images. Bone, 2014. 60: p. 172–85. [PubMed: 24334189]
19. Halleux C, et al. , Isolation of mouse osteocytes using cell fractionation for gene expression analysis. Methods Mol Biol, 2012. 816: p. 55–66. [PubMed: 22130922]

20. Mazur CM, et al. , Osteocyte dysfunction promotes osteoarthritis through MMP13-dependent suppression of subchondral bone homeostasis. Bone Res, 2019. 7: p. 34. [PubMed: 31700695]
21. Livak KJ and Schmittgen TD, Analysis of relative gene expression data using real-time quantitative PCR and the 2(-Delta Delta C(T)) Method. Methods, 2001. 25(4): p. 402–8. [PubMed: 11846609]
22. Tang SY, et al. , Matrix metalloproteinase-13 is required for osteocytic perilacunar remodeling and maintains bone fracture resistance. J Bone Miner Res, 2012. 27(9): p. 1936–50. [PubMed: 22549931]
23. Qing H and Bonewald LF, Osteocyte remodeling of the perilacunar and pericanalicular matrix. International journal of oral science, 2009. 1(2): p. 59–65. [PubMed: 20687297]
24. Xiong J and O'Brien CA, Osteocyte RANKL: new insights into the control of bone remodeling. Journal of bone and mineral research : the official journal of the American Society for Bone and Mineral Research, 2012. 27(3): p. 499–505.
25. Bonewald LF, The amazing osteocyte. Journal of bone and mineral research : the official journal of the American Society for Bone and Mineral Research, 2011. 26(2): p. 229–238.
26. Dobin A, et al. , STAR: ultrafast universal RNA-seq aligner. Bioinformatics, 2012. 29(1): p. 15–21. [PubMed: 23104886]
27. Risso D, et al. , Normalization of RNA-seq data using factor analysis of control genes or samples. Nat Biotechnol, 2014. 32(9): p. 896–902. [PubMed: 25150836]
28. Robinson MD, McCarthy DJ, and Smyth GK, edgeR: a Bioconductor package for differential expression analysis of digital gene expression data. Bioinformatics, 2010. 26(1): p. 139–40. [PubMed: 19910308]
29. Stapleton M, et al. , Development of Bone Targeting Drugs. International journal of molecular sciences, 2017. 18(7): p. 1345.
30. Deal C, Potential new drug targets for osteoporosis. Nat Clin Pract Rheumatol, 2009. 5(1): p. 20–7. [PubMed: 19098925]
31. Rochefort GY, Pallu S, and Benhamou CL, Osteocyte: the unrecognized side of bone tissue. Osteoporosis International, 2010. 21(9): p. 1457–1469. [PubMed: 20204595]
32. Alliston T, Biological regulation of bone quality. Current osteoporosis reports, 2014. 12(3): p. 366–375. [PubMed: 24894149]
33. Yee CS, et al. , Investigating Osteocytic Perilacunar/Canalicular Remodeling. Current Osteoporosis Reports, 2019. 17(4): p. 157–168. [PubMed: 31227998]
34. Aarden EM, Burger EH, and Nijweide PJ, Function of osteocytes in bone. J Cell Biochem, 1994. 55(3): p. 287–99. [PubMed: 7962159]
35. Dole NS, et al. , Osteocyte-Intrinsic TGF-beta Signaling Regulates Bone Quality through Perilacunar/Canalicular Remodeling. Cell Rep, 2017. 21(9): p. 2585–2596. [PubMed: 29186693]
36. Fowler TW, et al. , Glucocorticoid suppression of osteocyte perilacunar remodeling is associated with subchondral bone degeneration in osteonecrosis. Scientific Reports, 2017. 7: p. 44618. [PubMed: 28327602]
37. Mueller M, et al. , A systemic acceleratory phenomenon (SAP) accompanies the regional acceleratory phenomenon (RAP) during healing of a bone defect in the rat. J Bone Miner Res, 1991. 6(4): p. 401–10. [PubMed: 1858523]
38. Schilling T, et al. , Influence of inflammation-mediated osteopenia on the regional acceleratory phenomenon and the systemic acceleratory phenomenon during healing of a bone defect in the rat. Calcif Tissue Int, 1998. 63(2): p. 160–6. [PubMed: 9685523]
39. Shuid AN, et al. , Effects of calcium supplements on fracture healing in a rat osteoporotic model. J Orthop Res, 2010. 28(12): p. 1651–6. [PubMed: 20572125]
40. Fischer V, et al. , Calcium and vitamin-D deficiency marginally impairs fracture healing but aggravates posttraumatic bone loss in osteoporotic mice. Sci Rep, 2017. 7(1): p. 7223. [PubMed: 28775273]

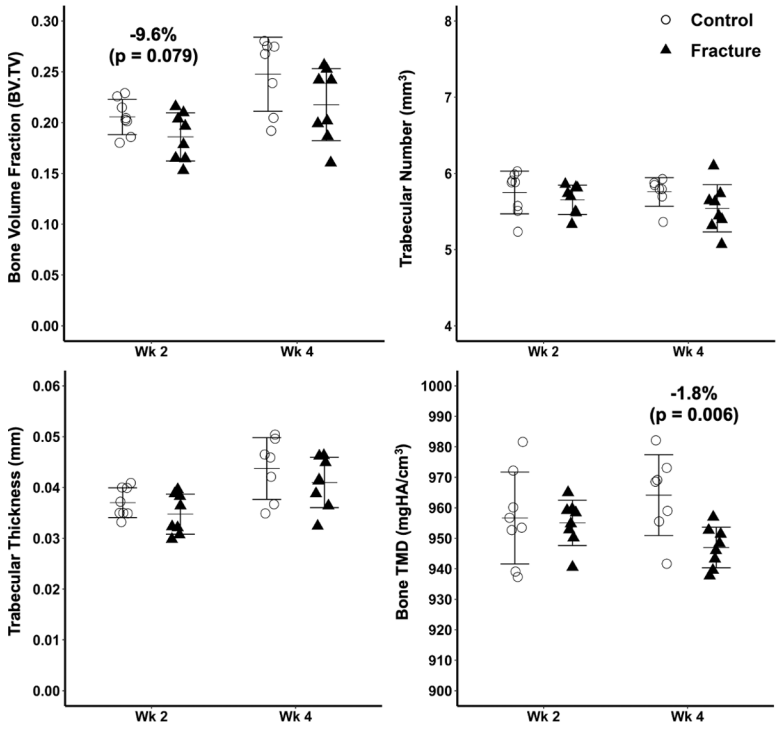

Figure 1.

Micro-computed tomography analysis of trabecular bone microstructure in the L5 vertebral body of mice at 2 and 4 weeks post-fracture (n=7–8 per group). Fracture was associated with decreased trabecular bone volume fraction (BV/TV) at this skeletal site, and significantly reduced bone TMD at 4 weeks post-fracture. Graphs show mean ± SD.

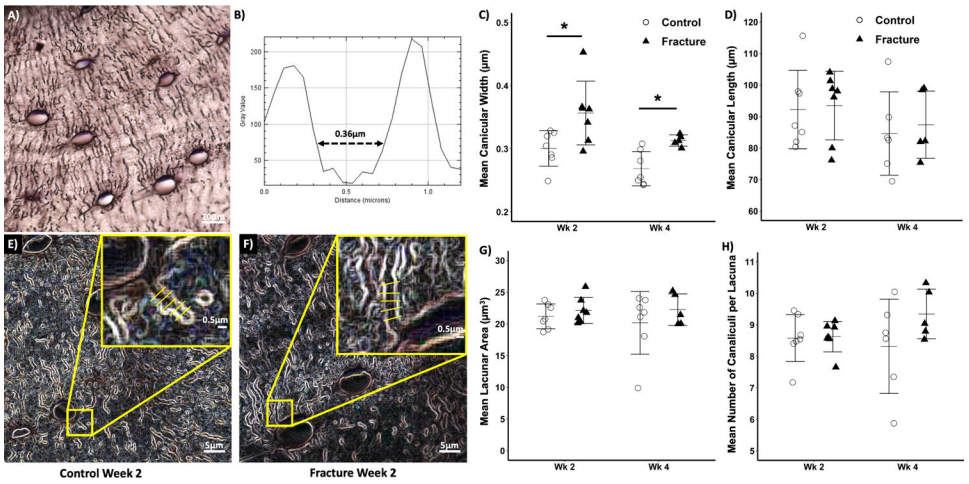

Figure 2.

Silver nitrate staining of transverse sections of the contralateral tibia. (A): Representative image of an unfiltered transverse section of cortical bone. (B): Grey value plot of lines drawn across canaliculi widths in the filtered images of (E-F). (E-F): Representative filtered images of canaliculi from (E) Control week 2 and (F) Fracture week 2 mice; yellow lines represent individual width measurements. (C): Mean canalicular width was significantly greater in the Fracture group at both week 2 and week 4 post-fracture. (D, G, H): No significant differences were observed between Fracture and Control mice for mean lacunar length (D), mean lacunar area (G), or mean number of canaliculi per lacuna (H). Graph shows mean ± SD, * denotes significant difference between Control and Fractured mice ($p \leq 0.05$).

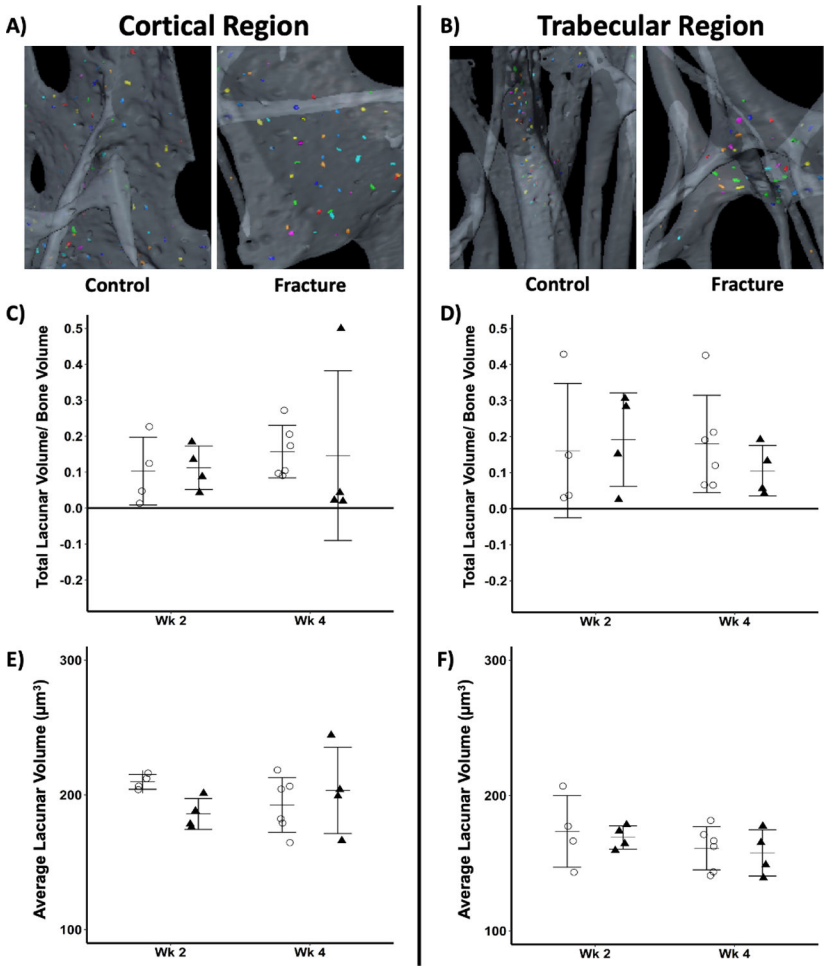

Figure 3.

High-resolution µCT of lacunar volume in cortical and trabecular bone at the proximal contralateral tibia. (A): Representative image of lacunae in cortical bone of Control and Fractured mice; (B) Representative image of lacunae in trabecular bone of Control and Fractured mice. Lacunae colors in these images are for visualization purposes only, and do not have any other meaning. (C-D): Total lacunar volume/bone volume in (C) cortical bone and (D) trabecular bone. (E-F) Average lacunar volume in (E) cortical bone and (F) trabecular bone. No significant differences were observed between Fractured and Control mice for either outcome at either of the time points. Graph shows mean ± SD.

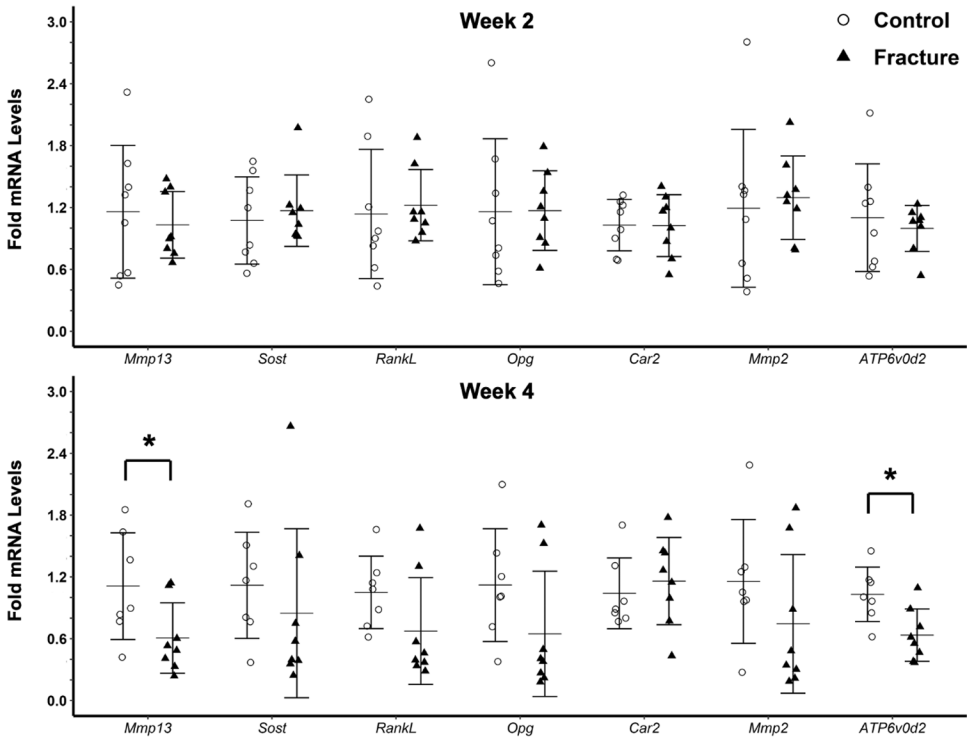

Figure 4.

RT-PCR analysis of genes associated with PLR in the contralateral femurs of Control and Fracture mice (fold mRNA levels relative to β-actin levels). (A): No significant differences were observed between Control and Fractured mice for any PLR-related genes at week 2. (B) At week 4, Fractured mice exhibited 45.3% and 38.4% lower expression of *Mmp13* and *ATP6v0d2*, respectively, compared to Control mice. Graph shows mean ± SD, * denotes significant difference between Fractured and Control mice ($p \leq 0.05$).

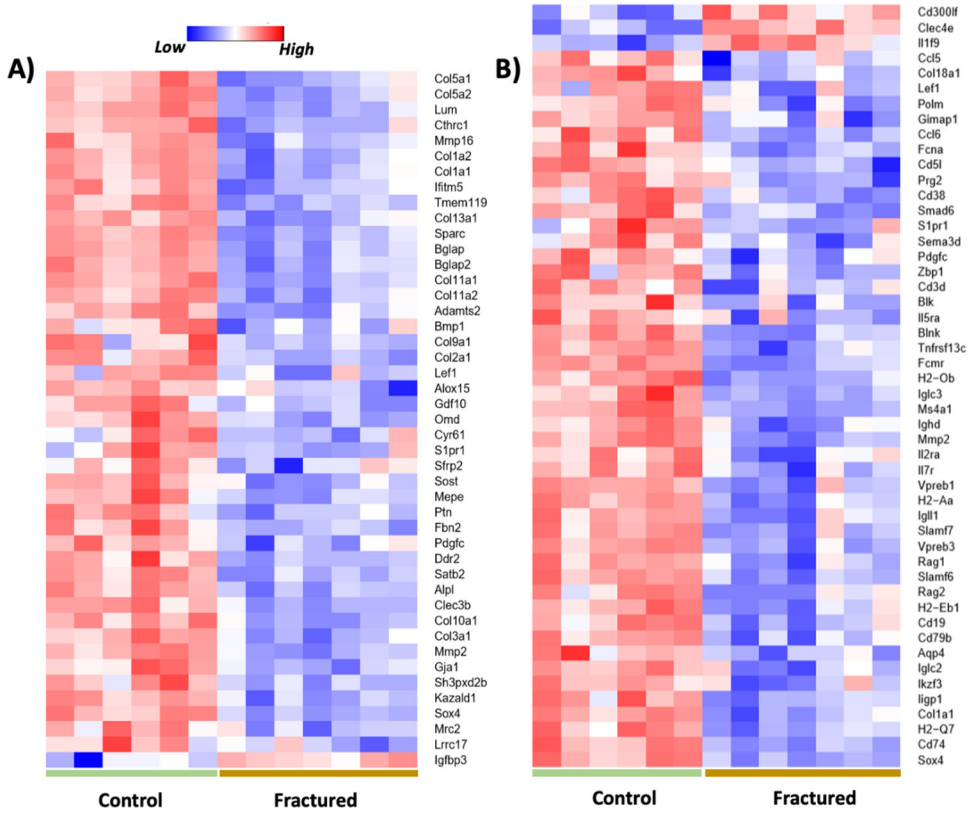

Figure 5.

Key genes identified as differentially expressed between Control and Fractured mice. (A): Skeletal development and bone metabolism-associated genes differentially expressed between Control and Fractured mice at day 3 post-fracture. (B) Immune/inflammatory response-related genes differentially expressed between Control and Fractured mice at day 3 post-fracture. The top 45–50 genes are shown in the heatmap.